



Multi-frequency, 3D ODS measurement by continuous scan laser Doppler vibrometry

Ben Weekes *¹, David Ewins ¹

University of Bristol, Queen's Building, University Walk, BS8 1TR, UK



ARTICLE INFO

Article history:

Received 5 December 2013

Received in revised form

8 May 2014

Accepted 30 December 2014

Available online 22 January 2015

Keywords:

Vibration

SLDV

3D

Scanning

Vibrometer

Velocity

ABSTRACT

Continuous scan laser Doppler vibrometry (CSLDV) is a technique which has been described and explored in the literature for over two decades, but remains niche compared to SLDV inspection by a series of discrete-point measurements. This is in part because of the unavoidable phenomenon of laser speckle, which deteriorates signal quality when velocity data is captured from a moving spot measurement. Further, applicability of CSLDV has typically been limited to line scans and rectangular areas by the application of sine, step, or ramp functions to the scanning mirrors which control the location of the measurement laser spot. In this paper it is shown that arbitrary functions to scan any area can easily be derived from a basic calibration routine, equivalent to the calibration performed in conventional discrete-point laser vibrometry. This is extended by performing the same scan path upon a test surface from three independent locations of the laser head, and decomposing the three sets of one-dimensional deflection shapes into a single set of three-dimensional deflection shapes. The test was performed with multi-sine excitation, yielding 34 operating deflection shapes from each scan.

© 2015 Elsevier Ltd. All rights reserved.

1. Introduction

Measurement of vibration fields by scanning laser Doppler vibrometer (SLDV) is commonplace, and a choice of commercial systems are available off-the-shelf. These systems have a host of advantages over conventional surface-mounted transducers like accelerometers, such as being non-contacting and allowing high spatial resolutions to be achieved. Within the field of vibration analysis, SLDVs are therefore an appealing choice for measurement of vibration on light and lightly-damped structures, the measurement of which is significantly affected by the presence of contacting instrumentation. SLDVs are optical interferometric devices comprising a single laser cavity and optical sensor, with the location of the measurement spot moved by scanning mirrors. However, as a SLDV is a single transducer, the vibration field is built from successive point measurements. This limits the speed at which a test of a high spatial resolution can be performed, with the desired bandwidth, and returned signal quality compounding the requisite capture time at each measurement location. There is a facility in some SLDV systems for 'fast scans' at a single excited frequency, in which an operating deflection shape (ODS) can be acquired rapidly due to the very limited number of samples required at each discrete measurement location. This manner of testing requires that the scanning mirrors quickly move the laser spot to the next measurement location. The inertia of

* Corresponding author.

E-mail addresses: B.Weekes@Bristol.ac.uk (B. Weekes), D.Ewins@Bristol.ac.uk (D. Ewins).

¹ Tel. +44 117 3315819.

the mirrors must therefore be considered, necessitating a dwell time to ensure the laser spot is at the intended measurement location and is stationary before capture starts. The dwell time can be minimised with low-inertia mirrors and feedback control, and it must be said that after several generations of the fast scan facility it is today highly optimised. However, this jerkiness seems fundamentally inefficient.

The experimental configuration of CSLDV described in this paper is optimised for rapid capture of high-resolution operating deflection shapes at multiple simultaneous excitation frequencies. The measurement spot is moved slowly and smoothly throughout the scan to minimise degradation of the velocity signal. Short windows of the time history can therefore be considered stationary, allowing conventional signal processing to be applied. This can be considered a compromise between typical SLDV and CSLDV, retaining merits from both approaches. By limiting the speed at which the laser-spot traverses the tested surface, the noise induced by laser speckle is minimised [1–5]. Laser speckle is a spatial phenomenon and so cannot be avoided in measurement by moving laser spot (assuming an optically-rough test surface, as is typical), but slow movement of the spot maximises the number of samples between speckles, and the associated signal drop-outs from the velocity decoder. With the assumption that the measurement point is stationary, the measurement bandwidth is maximised, i.e., for a test specimen which can be assumed to have a linear response to vibration, each frequency component in the measured velocity time history can be considered independent. There is a compromise between the speed at which the spot moves on the sample and the signal quality which can be achieved, but this is also a function of a large number of application-specific factors such as the SLDV employed, the focused spot size, the surface finish, the distance to the test surface, etc., many of these factors even varying within a single test. An experimental pre-test routine could usefully be derived to aid selection of the test parameters, but this is not explored here.

Note that most efforts in CSLDV to date have focused on relatively high scan rates, often scanning back and forth along a linear path, e.g., [6,7]. This approach has definite benefits for impulse-type excitation, which is often the best choice when a free-free test is desired. However, the scan rates that can be achieved are limited by the inertia of the mirrors and deterioration of the signal due to laser speckle, making area scans with impulse excitation applicable only to very lightly damped structures [7]. Accepting this fundamental difficulty of impact excitation applied to area scans, the simplistic processing employed in this report is tailored to continuous excitation using a shaker. This slow continuous scan paradigm also avoids the need to compensate for the inertial effects of the mirrors, which typically manifests as a reduction in the size of the scan area and a phase lag (for sinusoidal scans) [8], and has been observed to require higher order terms to correct at high scan rates [6].

2. Theory

2.1. Extension of CSLDV to non-planar/non-rectangular areas

Historically, continuous scan LDV inspections have typically been performed by controlling the scanning mirrors with function generators (typically sine or a combination of ramp/step functions), therefore limiting the inspection to 1D line scans, or scans of 2D rectangular areas on approximately planar surfaces. In this report the scanning mirrors are controlled using arbitrary functions created using knowledge of the tested surface, thereby permitting inspection of more complicated topologies. An example of an arbitrary scan path on a holed steel plate is given in Fig. 1. A frame from the video feed is shown in this Figure, from which a user-generated binary image was created. A scan path analogous to CNC pocket milling was automatically created from the binary image using a bespoke algorithm, and an example ODS using the scan path is given. The calibration and data-processing for this example were as described in this report, albeit as a single SLDV test case (i.e., 1D measurement) without range-finding.

The specimen considered for 3D CSLDV in this report was bent from a $100 \times 220 \text{ mm}^2$ steel plate and so can easily be considered as a mapping of a rectangular surface, permitting use of a Lissajous trajectory as a convenient area scan. However, the presented mathematics are generalised such that non-rectangular geometries like the example given in Fig. 1 can be inspected using a tailored scan path. Ewins et al. [1, 9] consider the area scanned by a Lissajous trajectory in normalised coordinates, i.e.:

$$n_x(t) = \cos \omega_{xt}; \quad n_y(t) = \cos \omega_{yt} \quad (1)$$

Analytical use of n_x and n_y is thereby eased by these simple functions, then typically progressing with the assumption that the measured velocity is normal to a planar surface upon which the laser-spot traces the Lissajous trajectory. The extension employed here retains the scanned surface $\langle n_x, n_y \rangle$, but considers it a parametric surface (as a function of time) in three-dimensional metric space; upon the surface the scan remains a Lissajous trajectory, but it is distorted to fit the three-dimensional surface geometry of the test-piece. Further, since the surface is characterised, the measurement direction need not be assumed to be aligned with a single nominal axis, which permits accurate reconstruction of the measured component of the ODS, and three independent velocity measurements to be resolved into orthogonal velocity components (see Section 2.2). The distorted Lissajous trajectory used in this paper can still be processed in the manner described by Ewins et al. to yield a table of polynomial coefficients describing the ODS measured by each SLDV, although for this processing method care must be taken to set the scan rates to control the spectral content of the velocity time-history, and limits are placed on the excitation [1]. In this paper a multi-sine excitation is used, which – since deterministic – allows a discrete Fourier transform to be applied. Successive short-time windows were considered with a window-size chosen such

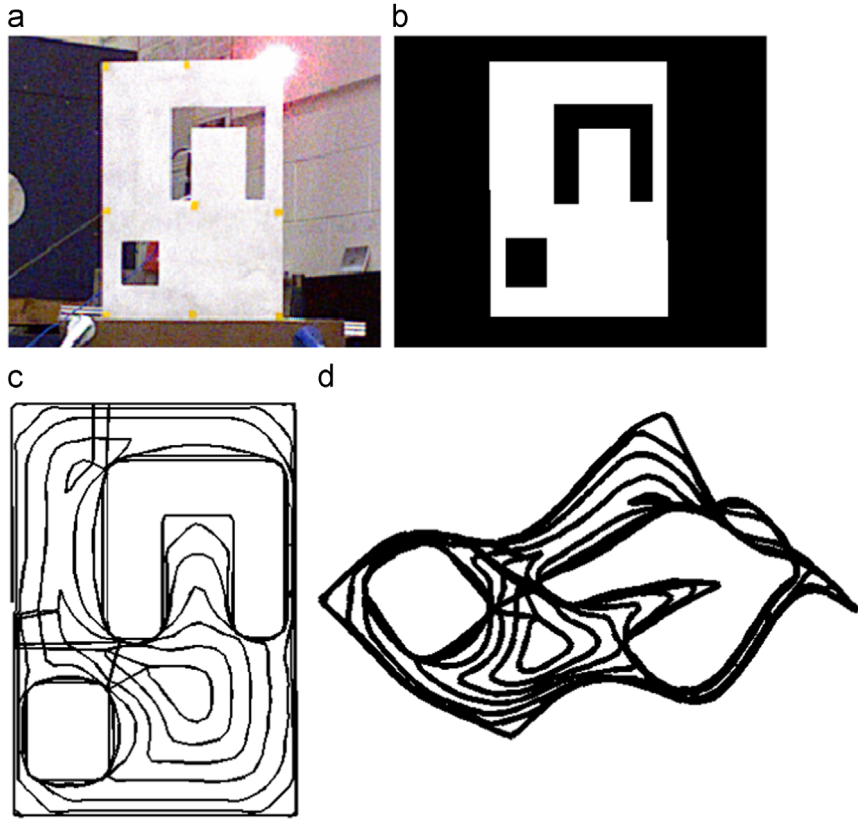


Fig. 1. Images illustrating the flexibility of the approach to CSLDV detailed in this paper. (a) Photograph of flat plate with complicated holes which the laser must avoid. (b) Binary image generated by drawing primitive shapes on the calibrated video feed. (c) Scan path generated using a CNC milling type methodology. (d) Resultant ODS at 352 Hz. This Figure care of F. Acciavatti, Masters Thesis, Marche Polytechnic University (pending, 2015).

that the frequency component of interest divided into the window an integer number of times, isolating the interrogated frequency to a single component in a discrete Fourier basis, e.g.:

$$v(\omega, m) = \frac{2WF}{N} \sum_{n=0}^{N-1} v(n+m-N/2)w(n)\exp(-j\omega[n+m-N/2]/F_s) \in C \quad (2)$$

Where WF is the window factor, v is the captured velocity time history, w is the window function, n and m are discrete indices, N is the window size and ω is the angular frequency of interest. n and m are zero-indexed indices, with m corresponding to the location of the windowing function. Note that the $-N/2$ terms centre the window on the new sampling index, m , and need rounding if N is odd. Use of this Equation is illustrated in Fig. 2, which shows an instance of a Hann window applied to the multi-sine signal captured in Section 4, in this case the sampling frequency being 83 kHz and the window length of 23,865 samples (≈ 0.29 s) designed to give 645 periods of the 2252 Hz excitation frequency of interest. The vectors n_x and n_y which describe the trajectory of the laser spot are resampled to conform to the new sampling index m , which can be set to overlap the considered windows of data if m is calculated at intervals of less than N . A forcing reference signal is evaluated in the same manner as the velocity signal to give a measure of complex mobility (i.e., velocity/force). This formulation is simply a selective short-time discrete Fourier transform, targeting specific frequency components, and so is independent of the specific scan path employed. This formulation is subject to the same compromise between the resolution of the frequency and time data as a spectrogram, dependent on the chosen window size. For rapid processing, ideally, a window-size is chosen such that all excited frequency components of interest divide into the window an integer number of times, and the frequency components of interest can be selected from a fast Fourier transform. However, when a large range of frequencies are excited this is not always practicable, necessitating different windowing for the different frequency ODSs which are to be extracted. Although a discrete Fourier approach is taken here employing a multi-sine excitation, an equivalent cross-power spectral density formulation can easily be substituted, and would allow use of random excitation (assuming a sufficiently slow scan rate). This short-time approach is extremely simple to implement, and has the benefit of localising the effects of noise such that spurious data-points can easily be discarded, e.g., by rolling-median filter. The effect of localising the noise is especially useful when laser speckle induces significant intermits in the signal, and it should be noted that after a significant signal intermit the velocity decoder can require time for the signal to stabilise again. This is potentially advantageous over methods which process the complete velocity time history in a single linear-regressive

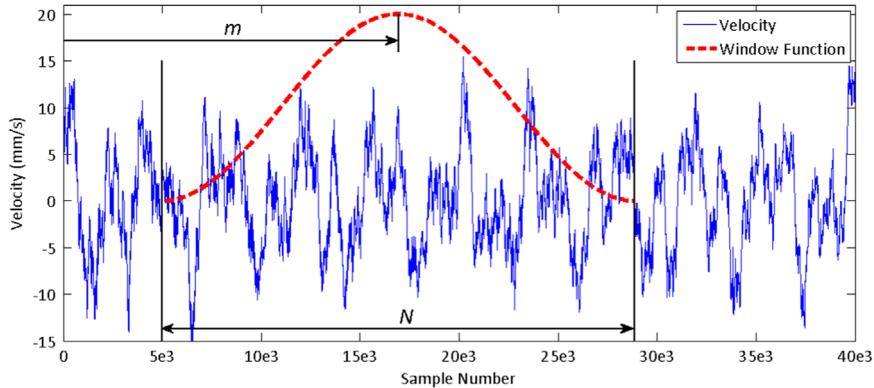


Fig. 2. Explanation plot to accompany Eq. (2). Successive short-time windows are considered, each of which are transformed into the frequency domain to give a discrete frequency component at index m . The pictured window function is arbitrarily scaled for illustrative purposes. Note that the sample numbering on the x -axis applies to the velocity time-history only, i.e., the window function indexing is always zero to $N - 1$. The velocity time-history shown was captured whilst employing a multi-sine excitation (from the test described in Section 4), hence the signal envelope is not as regular as is often observed for single-frequency CSLDV velocity signals.

operation, which can be dangerous when the signal is polluted by biased artefacts of the velocity decoder as a consequence of low levels of returned laser light. In instances when the velocity signal is poor (e.g., low levels of the laser light returned by the scanned surface) the ODS takes a chaotic form visually similar to a ‘cloud of flies’, which unambiguously indicates the deficiency of the captured signal. This is advantageous over processing methods which assume a low polynomial order as a description of the ODS, where such a deficiency may not be obvious just from observing the ODS. Further, since this processing method requires no assumptions about the spatial order of the ODS, the spatial resolution is limited only by the speed at which the laser spot moves and the size of the window, which should be set such that the distance traversed by the laser spot during the window is acceptably small. Discontinuities in the vibration shapes can therefore be ably detected by this method. The window size can be adapted to the frequency of excitation since lower frequencies of excitation will see fewer cycles of the excitation for a given temporal window length, but will also tend to be of a lower spatial order relative to the spatial window length. It is notable that since windows of the time history are considered, a pseudo real-time output can be realised as the scan is performed.

For alternative approaches to the interpretation of CSLDV data see, e.g., [10] for a discussion of Fourier series type approach, demodulation, and the Hilbert transform, [11] for time domain linear regression to yield polynomial coefficients, and [6] for further commentary on Fourier series and for the ‘lifting’ method.

2.2. Mapping of the tested surface

The geometry of the parametric test surface, X , is defined in standard three-dimensional Euclidean space:

$$X(n_x, n_y) = (x(n_x, n_y), y(n_x, n_y), z(n_x, n_y)); \quad X \in E^3 \begin{cases} -1 \leq n_x \leq 1 \\ -1 \leq n_y \leq 1 \end{cases} \quad (3)$$

In the case study detailed in this paper the scanned surface was smooth and so the simple topology was easily mapped onto a continuous, smooth surface in three-dimensional space as low-order, bivariate polynomial functions of the normalised 2D coordinate space $\langle n_x, n_y \rangle$:

$$x(n_x, n_y) = \sum_{j=0}^M \sum_{i=0}^N a_{ij} f_i(n_x) f_j(n_y) \quad (4)$$

Where $f_i(x)$ is the polynomial operator of degree i , and $y(n_x, n_y)$ and $z(n_x, n_y)$ are defined equivalently to $x(n_x, n_y)$. The values a_{ij} were found for x, y, z , by pseudo-inversion of appropriate Vandermonde matrices using data from a set of calibration points, e.g.:

$$\begin{Bmatrix} a_{00} \\ a_{01} \\ \vdots \\ a_{10} \\ \vdots \end{Bmatrix} = \begin{bmatrix} f_0(n_{x1})f_0(n_{y1}) & f_0(n_{x1})f_1(n_{y1}) & \dots & f_1(n_{x1})f_0(n_{y1}) & \dots \\ f_0(n_{x2})f_0(n_{y2}) & f_0(n_{x2})f_1(n_{y2}) & \dots & f_1(n_{x2})f_0(n_{y2}) & \dots \\ \vdots & \vdots & & \vdots & \dots \end{bmatrix}^+ \begin{Bmatrix} x_1 \\ x_2 \\ \vdots \end{Bmatrix} \quad (5)$$

Note that the parametric surface described by $\langle n_x, n_y \rangle$ need not be normalised to the interval -1 to 1 as defined in Eq. (3) and can be any convenient (consistent) system, but in retaining the normalisation, the processing by Ewins et al. can be retained. The normalised interval also gives a greater number of options if a polynomial basis for the description of the tested surface

is chosen (e.g., Chebyshev), which can be advantageous since the description of the surface may be better described with fewer terms in a particular polynomial basis, minimising the rippling phenomenon often observed in high-order polynomial descriptions known as Runge's phenomenon.

Also note that the inverse mapping from X to $\langle n_x, n_y \rangle$ need not be unique – it may be useful in some cases to make two neighbouring corners of a 2D Lissajous trajectory coincident to form a scan of a triangle for later tessellation, e.g., where the surface is highly angular and is best suited to a series of local scans. For more geometrically-complex surfaces, piecewise functions such as splines may be required for an accurate mapping. The requirement for a precise description of the surface is somewhat relaxed by the minimal demands put upon it, consider:

- 1) The calibration points on the test surface which are used to estimate the relative location of the test surface and SLDV head are the same for each SLDV head. The calibration points are also used to approximate the surface, and so estimation of the relative location of the SLDV head and test surface is relatively independent of the interpolation of the surface (see [Section 2.4](#)).
- 2) The vectors $\hat{l}_1, \hat{l}_2, \hat{l}_3$ used to describe the velocity measurement directions at each measurement location are relatively insensitive to small errors in the description of the measured surface topology since the distance between the SLDV and the test-piece is typically considerably larger than the scale of the test-piece geometry.
- 3) If the scan paths on the tested surface are seen to be locally equivalent and the capture buffers are synchronised, the measurement locations are adequately described in terms of $\langle n_x, n_y \rangle$, i.e., the voltages sent to the scanning mirrors, V_x and V_y , are defined as functions of the normalised surface coordinates only (Eq. (9)).
- 4) If the test data is to be correlated against modelled data, the error in the approximation of the test geometry is typically on the order of the error in pairing test points and model nodes.

The method given here is primarily useful for surface topologies which can be described by a low order bivariate polynomial, since some effort is required in assigning the calibration points values on the normalised surface. If this method is to be used for highly geometrically-complex shapes a more automated approach is desirable since many calibration points would be required. However, given that a geometrically complex surface will typically fail to allow the unobstructed line-of-sight each SLDV head requires, this does not add significant constraint to the CSLDV method over use of SLDV in general. In some test cases it may be most expedient to split highly faceted test-surfaces into simpler sub-surfaces.

2.3. Extension of CSLDV from one to three dimensions

An LDV measures velocity at the laser spot, in the direction of the beam of the laser. Three LDVs trained upon a single measurement spot therefore yield three independent unit vectors for the respective measurement directions: $\hat{l}_1, \hat{l}_2, \hat{l}_3$. The measurements can therefore be decomposed into global Cartesian axes in the time or frequency domain thus:

$$\begin{Bmatrix} v_x \\ v_y \\ v_z \end{Bmatrix} = \begin{bmatrix} \hat{l}_1^T \\ \hat{l}_2^T \\ \hat{l}_3^T \end{bmatrix}^{-1} \begin{Bmatrix} v_1 \\ v_2 \\ v_3 \end{Bmatrix} \quad (6)$$

Where the respective velocity components, v , may be time or frequency domain data (provided they are consistently defined). From Eq. (6) it is clear that the LDVs should be located with measurement directions that yield a well-conditioned matrix for accurate inversion. When using mirrors to deflect the measurement location on the tested surface, the unit vectors $\hat{l}_1, \hat{l}_2, \hat{l}_3$ for the respective SLDVs vary, and so there is a unique matrix for each measurement location. In this report a single SLDV head was employed for each independent view of the surface by moving the head after each scan, and so acquisition of the three velocity components was not simultaneous. This approach therefore necessitates correction of the phase of the velocity signal relative to the force reference before application of Eq. (6). Alternatively, the velocity terms in Eq. (6) can be substituted for respective complex mobility components. For each position of the SLDV head the scan paths with respect to the tested surface were notionally identical, as were the acquisition rates and buffer lengths. It was therefore assumed that the location of the laser spot in each respective sample of the three velocity time histories was the same (mislocation of the spot due to the inertial effects of the scanning mirrors was neglected given the relatively slow speed at which the laser-spot was moved).

It is often useful to consider the three velocity components in local coordinate systems with respect to the inspected surface, i.e., two in-plane components (not necessarily orthogonal) and a surface-normal, i.e.:

$$\mathbf{u}_x = \frac{\partial X}{\partial n_x}; \quad \mathbf{u}_y = \frac{\partial X}{\partial n_y}; \quad \hat{\mathbf{u}}_z = \hat{\mathbf{u}}_x \times \hat{\mathbf{u}}_y \quad (7)$$

Where the hat accent denotes a unit vector. Calculation of the local in-plane and out-of-plane components can be performed easily if the test surface is continuously and smoothly mapped (e.g., by polynomial function, [Section 2.2](#)). The equation to

decompose the three velocity datasets (in temporal or frequency domains) then becomes:

$$\begin{Bmatrix} v_{\mathbf{u}_x} \\ v_{\mathbf{u}_y} \\ v_{\mathbf{u}_z} \end{Bmatrix} = \left[\begin{Bmatrix} \hat{l}_1 \\ \hat{l}_2 \\ \hat{l}_3 \end{Bmatrix} \begin{Bmatrix} \hat{\mathbf{u}}_x \\ \hat{\mathbf{u}}_y \\ \hat{\mathbf{u}}_z \end{Bmatrix}^T \right]^{-1} \begin{Bmatrix} v_1 \\ v_2 \\ v_3 \end{Bmatrix} \quad (8)$$

2.4. Calibration routine

2.4.1. Scanning mirrors

The laser spot can be located accurately on the test surface by relating the voltages which drive the scanning mirrors directly to the normalised surface, i.e.:

$$V(n_x, n_y) = (V_x(n_x, n_y), V_y(n_x, n_y)) \quad (9)$$

Where V_x and V_y are the voltages sent to the two scanning mirrors. A series of calibration points are defined in normalised coordinates around the periphery and upon the scanned surface to achieve this mapping. Such a set of calibration points also implicitly corrects for the field distortion caused by inter-dependence of the scanning mirrors.² This pragmatic approach of test-specific calibration of the scanning mirrors and the test surface is typical of all SLDV systems which use a video feed, but in the configuration detailed in this report the calibration points also serve to form the geometry of the tested surface (Section 2.2), and estimate the relative location of the test surface and SLDV head (Section 2.3). The number of calibration points required is dependent on the complexity of the surface to be scanned. In the case study given in this report the voltages were characterised as a low-order polynomial, equivalent to the description of the surface itself in three-dimensional metric space (Equation (4)).

2.4.2. Local and global metric spaces

To find the measurement directions a rangefinder was attached to the SLDV head (see Section 2.4.3), and so the rangefinder moved with the SLDV head to each of the three viewpoints of the test surface. It was therefore necessary to transform between the local coordinates from the rangefinder to a global coordinate system in which $\hat{l}_1, \hat{l}_2, \hat{l}_3$ are defined. The transformation is simply:

$$\{X'\} = [R|T] \begin{Bmatrix} X \\ 1 \end{Bmatrix} \quad (10)$$

Where X and X' are points on the test surface in the respective coordinate systems, R is the 3×3 rotation matrix and T is the 3×1 translation matrix. Here, the global coordinate system was taken as the local coordinate system for the first location of the SLDV head. Finding the rotation and translation terms to map between coordinate systems is a common problem in robotics to which there are many solutions, the method used here by the author being based on singular value decomposition [12].

2.4.3. Microsoft Kinect-specific calibration

Commercially-available SLDV systems with range-finding typically use a time-of-flight laser sensor, with the range-finding laser sent through the same scanning mirrors used to steer the velocity measurement laser. This confers the advantage that in a well-calibrated system the location of each distance measurement is coincident with its respective velocity measurement, but typically requires that the optical system is mechanically split to share the scanning mirrors (use of semi-silvered mirrors would be detrimental to both velocity and distance sensing). As such, the range-finding procedure is protracted since the acquisition is non-concurrent. Alternatively, the commercial systems can also triangulate the measurement positions by knowledge of the angles through which the laser has been steered by the scanning mirrors, requiring no dedicated range-finding sensor. However, this approach requires accurate characterisation of the scan fields, and an extended manual calibration to check co-location the laser spots from the three SLDVs at each measurement point.

The Microsoft Kinect is an inexpensive piece of consumer-grade hardware, and is employed here for its range-finding functionality. The Kinect has two video sensors: one colour, and the other near-infrared. An infrared speckle pattern is projected onto the test surface by the Kinect which is seen by the infrared camera (Fig. 3), and by comparison with a reference speckle pattern triangulates the depth information [13]. Studies of the accuracy and sensitivity of the Kinect have been reported in [13–15], and it is observed to compare favourably with more expensive commercial systems at short ranges (< 3 m) [14,15]. For the purposes of this report the Kinect can be substituted for any other relatively accurate range-finding capability, provided it can be reconciled with the SLDV and the measurement locations. However, it should be noted that the combined colour and depth video streams from the Kinect provide additional data that can be beneficial in record-keeping and visualisation of the vibration fields.

² The location of the laser spot on the second scanning mirror varies as a function of the first scanning mirror, and so some pincushion distortion of the SLDV inspection field in one axis is typical.

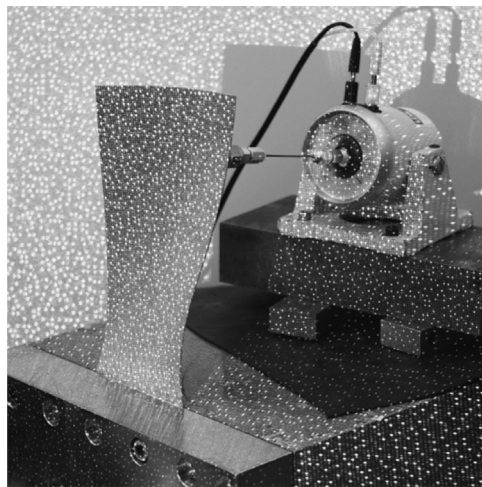


Fig. 3. Infrared photograph showing the speckle pattern used by the Microsoft Kinect for its range-finding facility. The infrared speckle pattern is compared to a reference speckle pattern to estimate the depth information. This calculation is performed within the Kinect (for how, see [14]), and full field depth images are outputted.

In order to combine the Kinect colour and depth video feeds, account must be taken for the separate imaging planes for the respective sensors. The association of the data from the colour and depth feeds is as follows:

$$K_d(i_d, j_d, z_d) \xrightarrow{\text{depth lens}} K_d(X_d(x_d, y_d, z_d)) \xrightarrow{\text{colour lens}} K_{d,c}(X_d(x_d, y_d, z_d), i_c, j_c, \text{RGB})$$

Where i and j are picture element (pixel) references, x, y, z , are the three orthogonal components in the metric space in which the surface X is defined, and the subscripts d and c are used to refer to which sensors (depth and colour respectively) inform the Kinect space. K .RGB refers to the respective red, green and blue colour channels. The pixels on the imaging plane of the depth camera ($K_d(i_d, j_d, z_d)$) were projected through the lens of the depth camera into metric space ($X_d(x_d, y_d, z_d)$), then through the lens of the colour camera onto the colour imaging plane ($K_c(i_c, j_c, \text{RGB})$). For correction of the distortions in the colour and infrared optics see [14]. A colour pixel was associated with each of the depth image pixels projected onto the colour imaging plane by a simple nearest-neighbour interpolation, this method chosen to minimise processing time to realise a near real-time output. Note that it is unnecessary to project back out through the colour lens into the metric space; it is only the association of colour information with the range-finding information which is performed on the colour image plane.

The test-surface data in the local Kinect metric space X_d , is transformed to the SLDV space, X , by use of Eq. (10). The rotation-translation matrix for this operation can be estimated by calibration using a planar target, set normal to the SLDV at a known distance (the target can be made planar to the SLDV by reflecting the laser back along its non-deflected ($V_x=0$, $V_y=0$) axis).

3. Test equipment

The test-piece employed in this paper was originally a $220 \times 100 \times 1$ mm steel plate, which was bent to resemble a turbine blade (hereon referred to simply as a blade). The blade was sand-blasted, then treated with grey primer and retro-reflective microspheres to maximise the back-scatter of laser light. The blade was clamped at one end, and excited via a stinger attached near the top of the blade (Fig. 4). Fifteen calibration points were marked on the blade in the form of a 3×5 grid using small squares of retro-reflective tape.

The SLDV system was a Polytec PSV-300, comprising a red HeNe (632.8 nm) laser with inbuilt scanning mirrors to steer the beam. The system is designed for discrete-point (stationary spot) measurements, and so it was largely bypassed: a National Instruments (NI) 9178 compactDAQ chassis with analogue voltage input and output cards (9205, 9263) captured the signals and controlled the scanning mirrors. The NI hardware was controlled using the Mathworks MATLAB signals acquisition toolbox. The NI hardware was also used to generate the multi-sine signal which was amplified and sent to the shaker.

The commercially-available three-dimensional SLDV systems comprise three SLDV heads to give the three independent views of each measurement location required to resolve the measured velocities into three orthogonal components Eq. (6). These three SLDV heads ideally have different Bragg cell frequencies such that any cross-talk is negligible (assuming the velocities encountered are reasonably modest). In the test configuration used in this paper only a single SLDV head was used, with the three independent observations of each measurement location performed sequentially, employing a phase reference (i.e., the force input). An SLDV head is a single transducer, and so SLDV field measurements are always built in a sequential fashion – the scope of such a test is therefore limited to repeatable velocity phenomena, particularly test-pieces

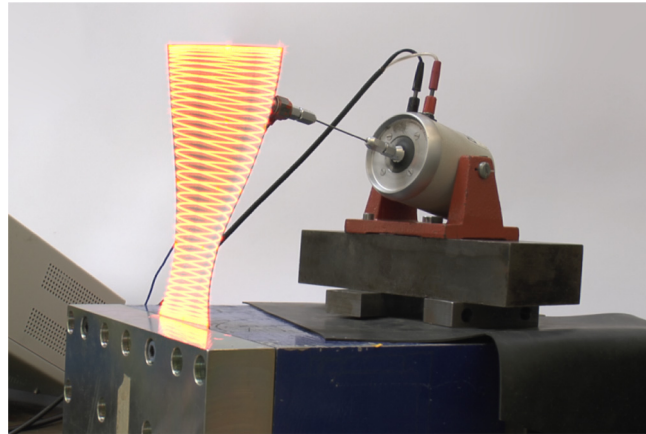


Fig. 4. Photograph of test piece in retention with excitation. The photograph is a long exposure to show the scan path.



Fig. 5. Photograph of Microsoft Kinect attached to Polytec SLDV laser head.

with an assumed linear vibration response. This limitation is also true of 3D SLDV systems, albeit the measurement may be concurrent at each respective measurement location.

For range-finding, a Microsoft Kinect was used, adhered to the SLDV head (Fig. 5). The Kinect was controlled using a bespoke Windows application written in C# using the Microsoft Kinect software development kit (SDK), and within the Mathworks MATLAB environment using the image acquisition toolbox. The Windows application was primarily used for pre-test calibration/characterisation of the Kinect since the OpenGL graphics facility was most efficient for displaying the three-dimensional metric space in near real-time. All capture of the Kinect data during the test was conveniently performed using MATLAB.

4. Test procedure

The SLDV head was placed in the first location, and calibrated to the blade using 15 calibration points marked on the blade with small squares of retro-reflective tape in a 3×5 grid. The calibration procedure required the user to guide the laser spot to each of the calibration points in turn, then press a button to log the voltages fed to the scanning mirrors and capture a number of colour and depth frames from the Microsoft Kinect (here, 20 frames for averaging). Once all calibration points had been logged this information was saved, and the user presented with a composite image comprising colour and depth information from all calibration points, as shown in Fig. 6. This composite image comprises the maximum intensity

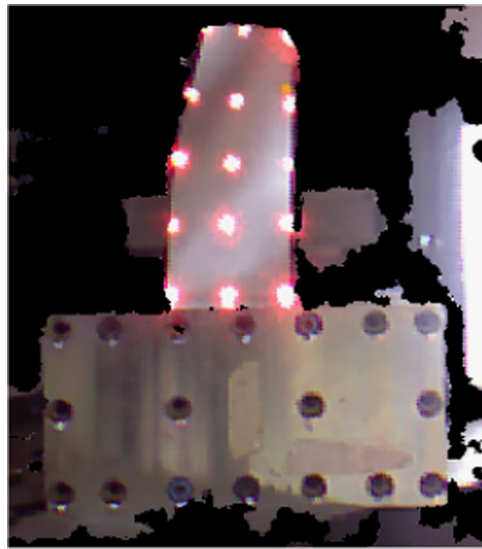


Fig. 6. Composite colour image showing the laser spot at each calibration point. Only pixels with associated depth information are shown, with black areas denoting no range information.

values from the acquired colour frames, with the colour pixels only given where there is associated depth information. By clicking on each of the spot locations in turn, the user defined the location of each of the calibration points in metric space, although this could be automated on a more developed system. Note that for the scan to be performed, only the relationship between the calibration points and the scanning mirrors need be known Eq. (9). The laser can be guided to the calibration points very accurately, and so for geometrically simple test-surfaces, generation of the scan path is not a cause of significant error. The software was written in such a way that the final step of locating the calibration points in the Kinect depth frame could be performed again *a posteriori* should there be any identified error, which was a potentially useful facility given the three successive calibration routines required for the single SLDV head used here.

In order to determine which frequencies were of interest, stepped-sine response functions were first taken at some of the calibration points, three of which are shown in Fig. 7. 34 frequencies were deemed of potential interest based on manual inspection of these response functions, and were combined to build a multi-sine excitation signal to be used in the continuous scan (these frequencies are given in Table 1). The excited frequencies were in the range 21–2252 Hz, and the mobility at these frequencies (measured at the calibration points) spanned over three orders of magnitude. The test was not optimised for the specific mobilities observed in the response functions, with the respective amplitudes of the sine components in the multi-sine signal all set equally. Note that at the higher frequencies included in the multi-sine signal the test-piece was significantly less mobile, and so signal quality worsened for higher frequency components, as can be observed in the stepped sine spectra. Scan rates of 76 cycles/buffer in the n_x direction and 3 cycles/buffer in the n_y direction were chosen to give a Lissajous trajectory with good coverage of the test surface and no redundancy (Fig. 8). This trajectory in the normalised surface space was mapped to the voltage plane of the scanning mirrors, yielding Fig. 9(a). As this was a reference dataset to prove and investigate the benefits of this method, the buffer was set generously to a length of 300 s and the maximum sampling rate available of 83 kHz. After the scan from the first location of the SLDV head was performed the SLDV head was moved to two further view-points, with calibration and test performed at each location. The corresponding outputted voltage planes are given in Fig. 9(b) and (c), and the reassembled range-finder data clouds from the respective SLDV locations in Fig. 10. In addition to the continuous scan data, discrete-point measurements using two seconds of the multi-sine excitation were taken at each of the 15 calibration points for the three locations of the SLDV head.

Since the scan was quite slow, the window size chosen in application of Eq. (2) was permitted to be in the range $\approx 0.2\text{--}1.3$ s, which with a 3/4 window overlap saw $\approx 900\text{--}4500$ data-points in the ODSs, each data-point having three degrees of freedom. Various window sizes were trialled, but for this test it was found empirically that a window of $0.28 \times f + 13$ cycles (rounded to the nearest integer) gave a good compromise between the spatial resolution of the ODS and the quality of the returned ODS.

5. Results and discussion

Figs. 11 and 12 show example ODSs at 21 Hz and 76 Hz respectively, viewed from various angles. The ODSs are observed to be extremely low-noise, and the number of data-points yielded by the continuous scan gives great ease in interpreting the deflection shapes. The 15 three-dimensional stationary reference points adequately describe these deflection shapes, but interpretation of even these low-order deflection shapes is aided by the increased spatial resolution of the continuous scan data. Further example ODSs are given in Fig. 13 from just the angle view-point. Although difficult to convey with static

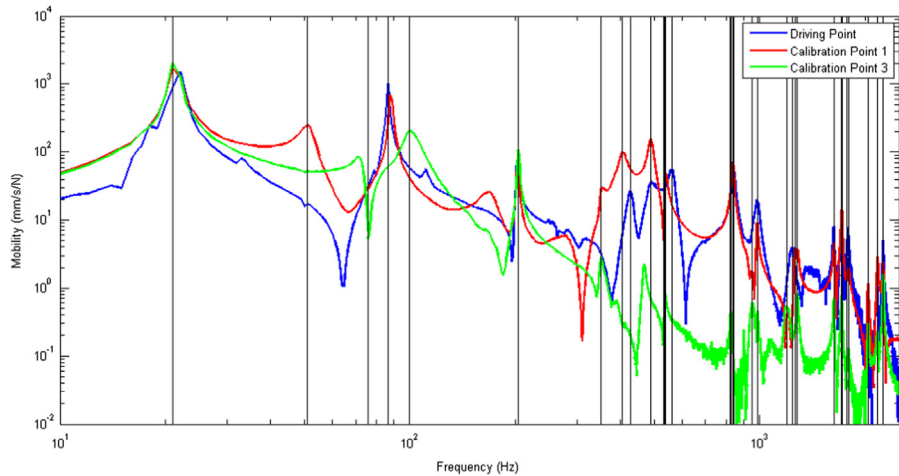


Fig. 7. Stepped sine mobility spectra for the driving point and two of the calibration points (top-left and top-right corners of the blade). The black lines mark frequencies included in the multi-sine excitation used in the continuous scan.

Table 1

Frequencies excited as part of the multi-sine excitation, and the correlation between the ODSs calculated from discrete-point measurements at the 15 calibration points and the continuous scan data.

Freq. #	Freq. (Hz)	Correlation (%)	Freq. #	Freq. (Hz)	Correlation (%)
1	21	99.5	18	842	99.0
2	51	99.6	19	950	98.0
3	76	99.9	20	984	98.9
4	87	99.9	21	1195	98.0
5	100	98.8	22	1238	97.2
6	204	99.5	23	1265	92.3
7	352	99.7	24	1280	95.5
8	405	99.4	25	1283	92.9
9	426	99.5	26	1627	96.7
10	488	99.3	27	1710	98.3
11	532	99.1	28	1716	98.3
12	535	98.7	29	1718	98.4
13	539	99.1	30	1772	98.5
14	561	99.3	31	1798	98.2
15	824	98.7	32	2038	98.9
16	829	99.1	33	2170	98.9
17	837	98.4	34	2252	99.3

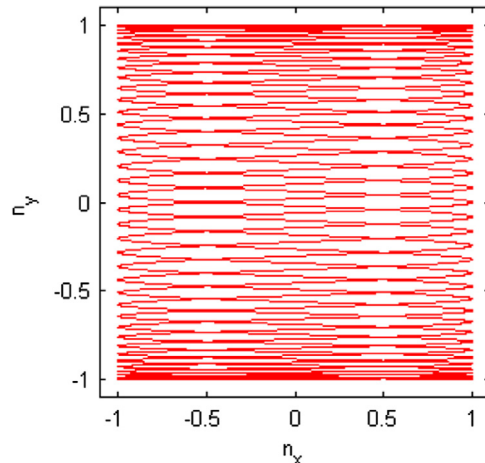


Fig. 8. The Lissajous trajectory used in the test, in the normalised coordinates upon the tested surface.

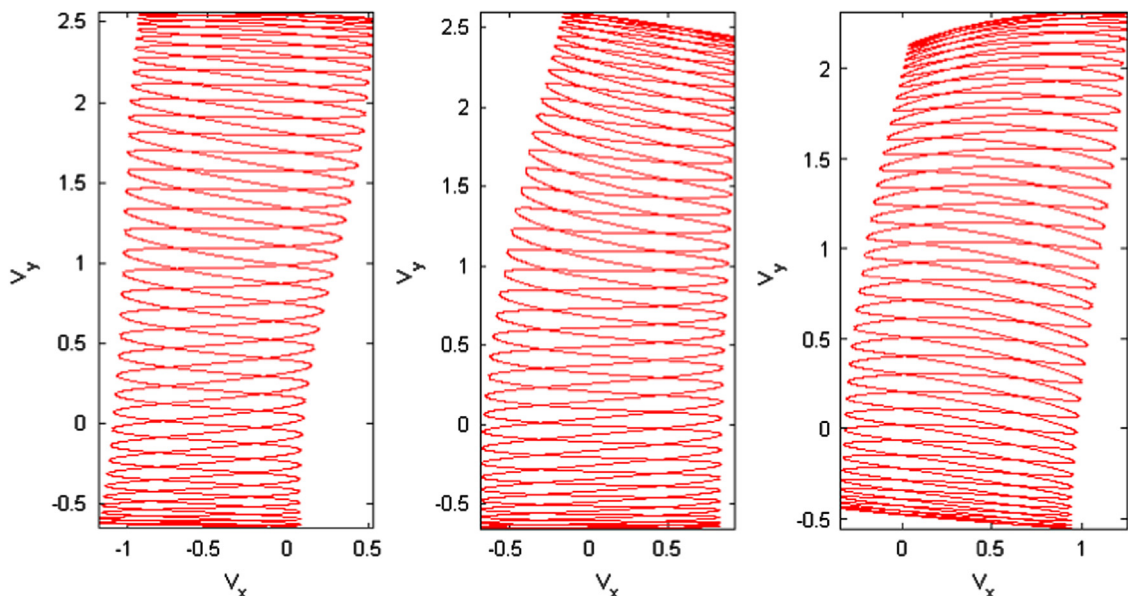


Fig. 9. Arbitrary functions applied to the scanning mirrors at the three respective locations of the SLDV head to achieve the correct local Lissajous trajectory upon the normalised surface (Fig. 8).

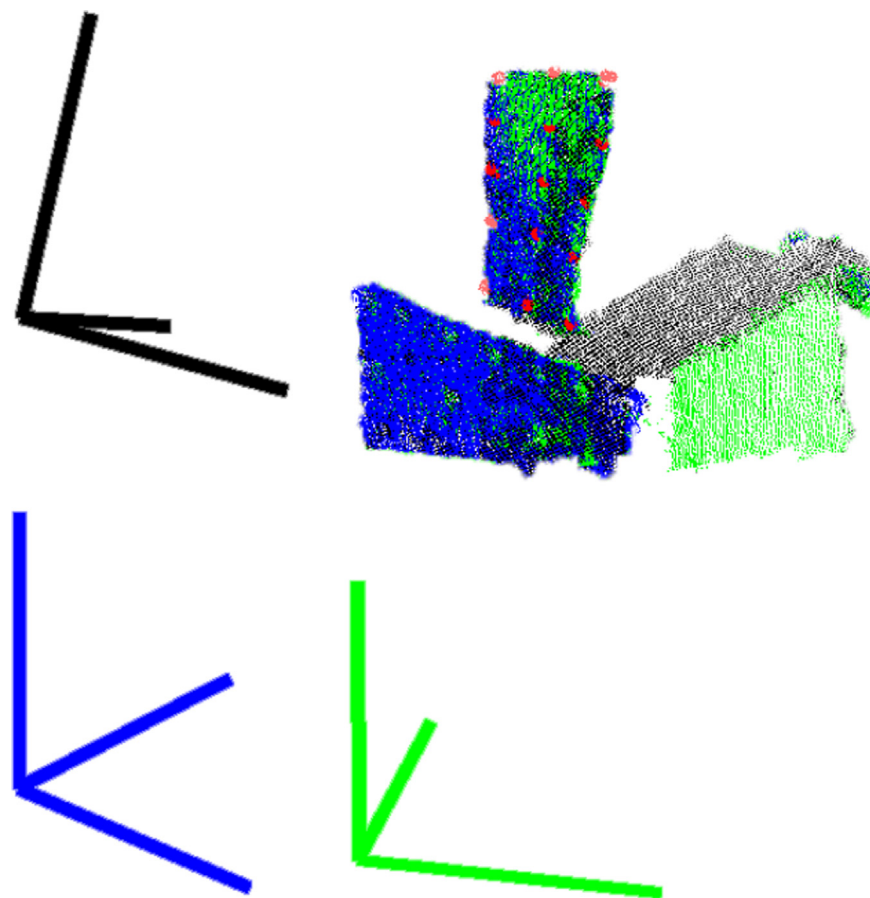


Fig. 10. Cloud of data-points comprising views from the three locations of the SLDV head within the master coordinate system. The blue, green and black data-points are from the respective locations of the SLDV head, with the corresponding coloured axes indicating the local coordinate systems. The red markers denote the calibration points (note there are three near-coincident markers corresponding to each of the respective SLDV head locations at each calibration point). (For interpretation of the references to colour in this figure legend, the reader is referred to the web version of this article.)

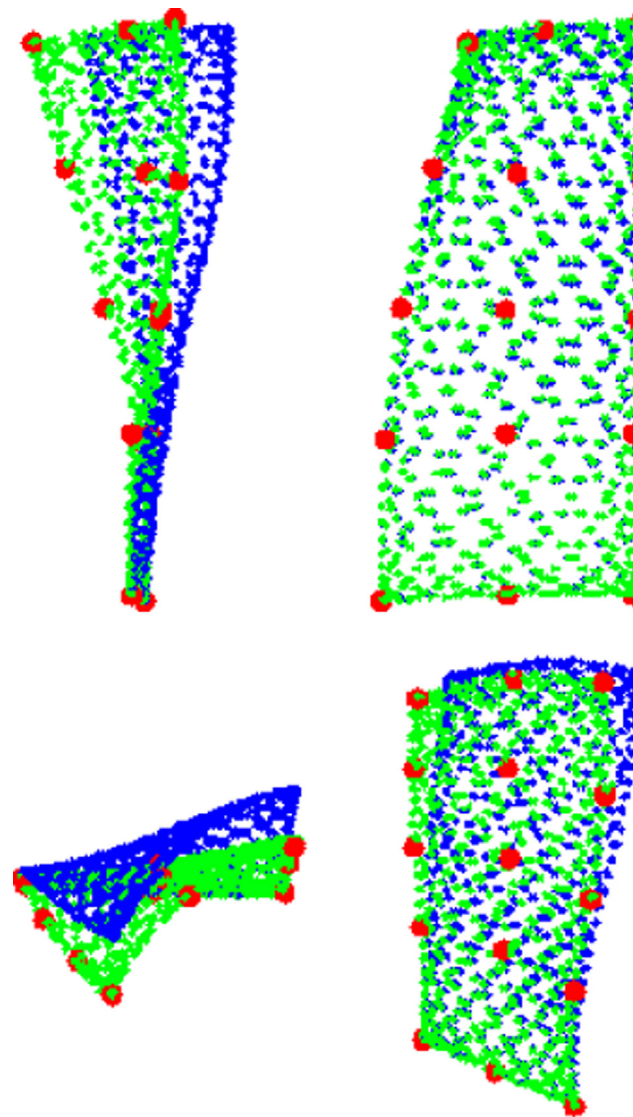


Fig. 11. ODS at 21 Hz, viewed (top-left) YZ, (top-right) XY, (bottom-left) XZ, (bottom-right) angle view. The blue points show the undeflected blade, the green points show the continuous scan ODS and the red points the reference discrete-point ODS taken at the calibration points. (For interpretation of the references to colour in this figure legend, the reader is referred to the web version of this article.)

images, these ODSs show benefit in the three-dimensional velocity data in this application, since the curved geometry of the blade exhibits ODSs which are highly three-dimensional, with various ‘unfurling’ type behaviours which could be interpreted as simple flexure with a one-dimensional measurement.

To compare the ODSs found by the continuous scan and the stationary point measurements, a correlation was performed using a normalised vector inner-product as is defined by the modal assurance criterion (MAC, [9]) for mode shape data. The correlation was performed between the 45 stationary point DOFs (i.e., 15 tri-axial measurements) and a median of neighbouring continuous scan data-points, the correlation values given in Fig. 14 and Table 1. The correlation is extremely high indicating consistent estimation of the ODS by both methods. This result is especially encouraging since the test-piece was rigidly clamped at the bottom, limiting the mobility of the lower part of the blade, and so the numerator of the correlation was effectively inhibited whilst any error inflates the denominator. It was also apparent that the regular grid of stationary reference locations was largely nodal for the ODSs around 1265–1283 Hz, which reduced the correlation since the stationary-point velocity signals were weak at these frequencies.

6. Conclusions

In this paper a methodology to extend continuous scan laser Doppler vibrometry to any arbitrary surface was given. Further, this capability was used to generate three-dimensional velocity data by repeated scans of the same area from

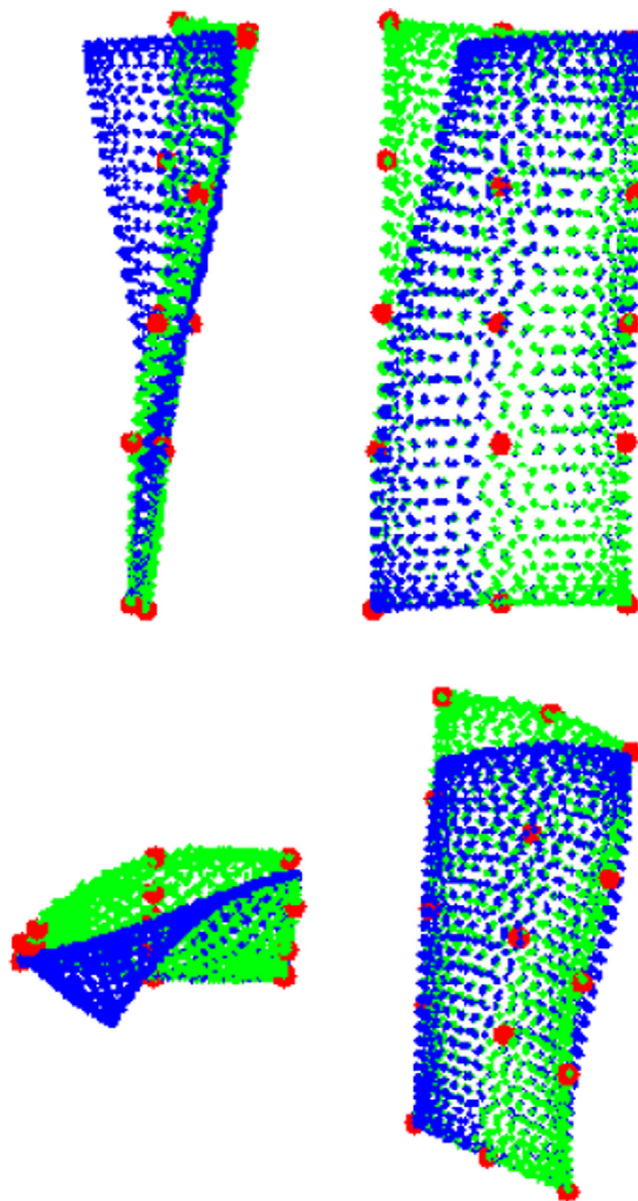


Fig. 12. ODS at 76 Hz, viewed (top-left) YZ, (top-right) XY, (bottom-left) XZ, (bottom-right) angle view. The blue points show the undeflected blade, the green points show the continuous scan ODS and the red points the reference discrete-point ODS taken at the calibration points. (For interpretation of the references to colour in this figure legend, the reader is referred to the web version of this article.)

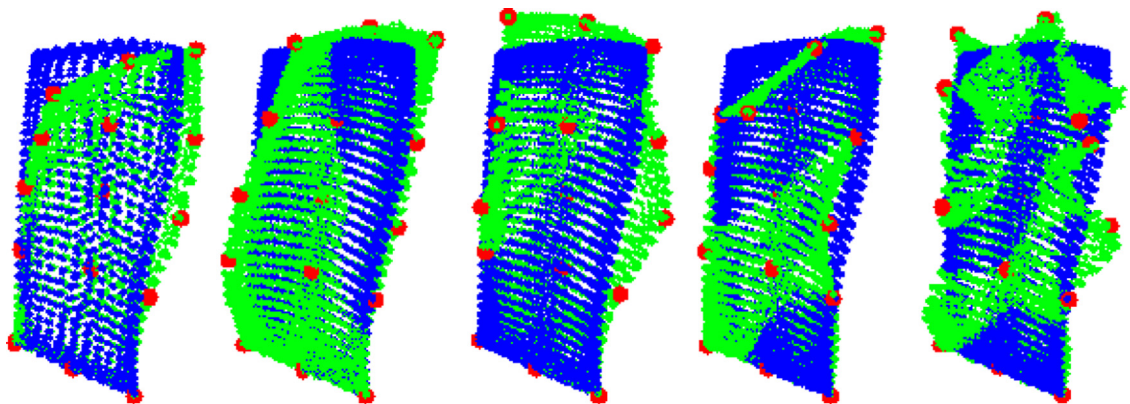


Fig. 13. Further example ODSs as per angle view in Fig. 12: (left-right) 100 Hz, 204 Hz, 352 Hz, 426 Hz, 2252 Hz.

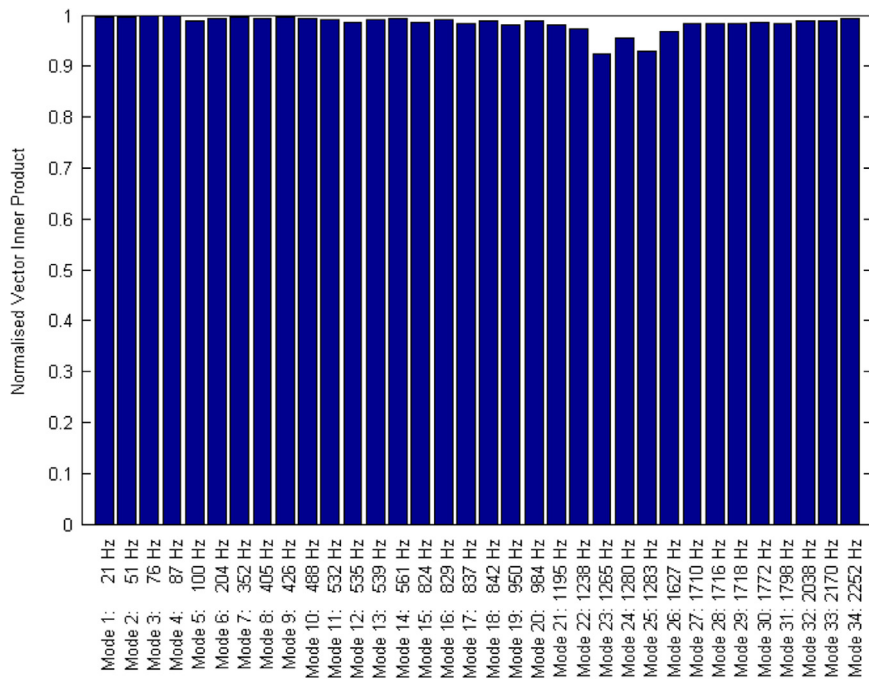


Fig. 14. Bar chart showing the agreement between stationary point measurements at the calibration points and the continuous scan data. 34 frequency components were excited.

different viewpoints, in what we believe to be the first demonstration of three-dimensional continuous scan vibrometry. The output from the test was 34 operational deflection shapes of a very high spatial resolution, captured simultaneously in a five minute scan. There remains significant room for optimisation and better understanding of the trade-off between scan length and the available excitation bandwidth, but even in this first realisation of this experimental configuration the results have been of a high quality and acquired within a reasonable time-frame.

Acknowledgements

This work was funded by the Technology Science Board for the Next-Generation Vertical Lift project, in collaboration with AgustaWestland NV. The authors would like to thank these respective institutions, without which this work would not have been possible.

Appendix A. Supporting information

Supplementary data associated with this article can be found in the online version at <http://dx.doi.org/10.1016/j.ymssp.2014.12.022>.

References

- [1] M. Martarelli, D. Ewins, Continuous scanning laser Doppler vibrometry and speckle noise occurrence, *Mech. Syst. Signal Process.* 20 (8) (2006) 2277–2289.
- [2] S. Rothberg, B. Halkon, Laser vibrometry meets laser speckle, in: Proceedings of the Sixth International Conference on Vibration Measurements by Laser Techniques: Advances and Applications, Ancona, Italy, 2004.
- [3] M. Sraric, M. Allen, Experimental investigation of the effect of speckle noise on continuous scan laser doppler vibrometer measurements, in: Proceedings of the IMAC XXVII, Orlando, Florida, 2009.
- [4] S. Rothberg, Laser vibrometry: pseudo-vibrations, *J. Sound Vib.* 135 (1989) 516–522.
- [5] S. Rothberg, Numerical simulation of speckle noise in laser vibrometry, *Appl. Opt.* 45 (2006) 4523–4533.
- [6] M. Allen, M. Sraric, A new method for processing impact excited continuous-scan laser Doppler vibrometer measurements, *Mech. Syst. Signal Process.* 24 (3) (2010) 721–735.
- [7] R. Ribichini, D. DiMaio, A. Stanbridge, D. Ewins, Impact testing with a continuously-scanning LDV, in: Proceedings of the IMAC-XXVI: Conference and Exposition on Structural Dynamics, Orlando, Florida, 2008.
- [8] D. DiMaio, SLDV Technology for Measurement of Mistuned Bladed Disk Vibration, Imperial College, London, 2007.
- [9] D. Ewins, Modal Testing 2, Research Studies Press Ltd., Hertfordshire, England, 2000.
- [10] M. Kang, A. Stanbridge, T. Chang, H. Kim, Measuring mode shapes with a continuously scanning laser vibrometer – Hilbert transform approach, *Mech. Syst. Signal Process.* 16 (2–3) (2002) 201–210.

- [11] I. Bucher, O. Wertheim, Measuring spatial vibration using continuous laser scanning, *Shock Vib.* 7 (2000) 203–208.
- [12] K.S. Arun, T.S. Huang, S.D. Blostein, Least-squares fitting of two 3D point sets, *IEEE Trans. Pattern Anal. Mach. Intell.* 9 (5) (1987) 698–700.
- [13] M. Anderson, T. Jensen, P. Lisouski, A. Mortensen, M. Hansen, T. Gregersen, P. Ahrendt, Kinect Depth Sensor Evaluation for Computer Vision Applications, Electrical and Computer Engineering, Technical Report ECE-TR-6, 2012.
- [14] K. Khoshelham, S. Elberink, Accuracy and resolution of kinect depth data for indoor mapping applications, *Sensors* 12 (2012) 1437–1454.
- [15] T. Stoyanov, A. Louloudi, H. Andreasson, A. Lilienthal, Comparative evaluation of range sensor accuracy in indoor environments, *Evaluation* (2011).